A quantitative study of the 7.7 and 11.3 micron emission bands based on IRAS/LRS spectra

Annie Zavagno, Pierre Cox, Jean-Paul Baluteau

Astron. Astrophys. 259, 241–251 (1992)

ASTRONOMY
AND
ASTROPHYSICS

A quantitative study of the 7.7 and 11.3 μm emission bands based on IRAS/LRS spectra

A. Zavagno[1], **P. Cox**[1,2], **J.-P. Baluteau**[1]

[1] Observatoire de Marseille, Place Leverrier, F-13248 Marseille Cedex 04, France
[2] Max-Planck-Institut für Radioastronomie, Auf dem Hügel 69, W-5300 Bonn 1, Federal Republic of Germany

Received April 30, 1991; accepted December 24, 1991

Abstract. This paper presents a quantitative analysis of the emission bands at 7.7 and 11.3 μm in the mid-infrared spectra of HII regions, reflection nebulae, planetary nebulae and galaxies. The study is based on a sample of 113 sources whose spectra have been extracted from the IRAS/LRS data base. Relations of the intensity of the emission bands with physical conditions such as the excitation, and the relative contributions of emission bands and continuum around 10 μm to the mid-infrared and far-infrared fluxes are presented and analyzed.

A strong linear correlation is found between the 7.7 and 11.3 μm band luminosities. The ratio of the 7.7 and 11.3 μm band intensities is equal to $8.3^{+3.8}_{-2.6}$. The good correlation and the small dispersion (30%, compatible with the measurement errors) confirm, on a large sample of sources, that the carriers of the 7.7 and 11.3 μm emission features belong to the same family, most likely aromatic molecular species such as PAH molecules. The average contribution of these features to the mid-infrared luminosity is 50%. The values range from 5 to 90 % where the smallest values are derived for sources with high excitation conditions. The contribution of the near-infrared emission bands to the total infrared luminosity is a few percent implying that one to five percent of the cosmic carbon is locked in the aromatic molecules. From simple energetical considerations, it is shown that the excitation of the 7.7 and 11.3 μm emission bands is dominated by ultraviolet photons in the range 365 to 91 nm.

Finally, the importance of the underlying continuum is stressed since it accounts, in a number of the sources, for more than half of the mid-infrared luminosity. However, the precise nature of its carriers is still unclear.

Key words: dust – infrared radiation – H II regions – reflection nebulae – planetary nebulae

1. Introduction

The study of small interstellar carbonaceous compounds has received increasing attention in the last ten years. An important reason for this interest has been the understanding of the basic mechanisms responsible for the set of interstellar infrared emission features at 3.28, 6.9, 7.7, 8.6 and 11.3 μm. The identification of these features with vibration modes of aromatic molecules attached to small carbon grains, suggested by Duley and Williams (1981), and the later extension of this suggestion to free Polycyclic Aromatic Hydrocarbons (PAHs) by Léger and Puget (1984) to account for the near-infrared studies of reflection nebulae by Sellgren et al. (1983) provided benchmarks for further investigations. Numerous laboratory studies and observational work have been done since then and detailed reviews are given in Puget and Léger (1989) and Allamandola et al. (1989).

PAHs have sizes (~ 1 nm) characteristic of big molecules and represent the upper molecular domain in the size distribution of interstellar grains. Another grain population, intermediate in size between the PAHs and the standard grains, is needed to explain the infrared emission observed longward of 15μm, and this component may also account for part of the emission at shorter wavelengths (see e.g. Désert et al., 1990). The precise relation between the smallest constituents of the carbonaceous particles and the somewhat larger compounds is still unknown, essentially because there is a lack of spectroscopic data at longer wavelengths. Clusters made of hydrogenated amorphous carbon (HAC) (Duley and Williams 1981) or Quenched Carbonaceous Composite (QCC) material (Sakata et al. 1984) are possible candidates for these intermediate size particles.

Small interstellar carbonaceous compounds (including both the PAH molecules and the larger cluster structures) are in many respects important constituents of the interstellar medium. The continuum plus the emission features of these particles account for about 30 to 40% of the infrared emission in the solar neighbourhood (Boulanger and Pérault, 1988) and represent a similar fraction of the integrated infrared luminosity of galaxies, including our own (Cox and Mezger, 1989 and references therein). These studies are based on the IRAS photometric data and consequently the relative contributions of the continuum and emission bands are not well known. The presence of aromatic molecules influences interstellar chemistry (Omont, 1986) and these small particles may have a key role in the heating of the interstellar gas (d'Hendecourt and Léger, 1988; Verstraete et al., 1990).

Studies of the PAH emission band strength have only been completed on a relatively small sample of sources. Cohen et al. (1986, 1989) published studies, based on airborne observations, of 22 northern and 18 southern sources, respectively. Emphasis was put on the 6.2 and 7.7 μm bands and the data of the IRAS/Low Resolution Spectrometer (LRS) were taken into account when available. Good correlations were found between the strengths of

Send offprint requests to: A. Zavagno

the emission bands at 6.2, 7.7 and 11.3 μm implying a common class of carriers for the features. The carbonaceous nature of the carriers was supported by the relation found between the intensity ratio of the 7.7 μm band relative to the far-infrared flux and the C/O ratio derived from optical data. More recently, Jourdain de Muizon et al. (1990b) analyzed the IRAS/LRS spectra of 24 sources in which they detected the 3.3 μm emission feature. The intensity ratio of the 11.3 μm to the 3.3 μm bands was used to put constraints on the average size of the molecular carriers which appears to be rather large, with 50 to 130 atoms.

The ubiquity of the emission bands at 7.7, 8.6 and 11.3 μm in the IRAS/LRS spectra (Jourdain de Muizon et al., 1990a) is a unique opportunity to study the quantitative behaviour of these bands on a large sample of sources spanning a wide range in physical conditions. Therefore, we present an analysis of the strength of the 7.7 and 11.3 μm bands in a sample of 113 sources including HII regions, reflection nebulae, planetary nebulae and galaxies. For most of the sources, the distance and the number of Lyman continuum photons are known, allowing a careful analysis of the band strengths as a function of physical conditions. The important questions of the contribution of the PAH emission bands to the mid-infrared luminosity and the relative contributions of emission bands and underlying continuum are also addressed and analyzed for the first time on a large sample of sources.

In Section 2, we describe the data, the selection criteria and the data reduction. In Section 3, we present the results of this study: the correlation between the luminosities of the 7.7 and 11.3 μm emission bands, their contribution to the mid-infrared luminosity and the dependence of this contribution on the excitation conditions. In Section 4, the results are discussed and the general conclusions are presented in Section 5.

2. Data reduction

2.1. Selection criteria

A detailed description of the IRAS Low Resolution Spectrometer (LRS) is given in Wildeman et al. (1983) and further information, particularly about the data reduction (calibration, average spectra) can be found in the IRAS Explanatory Supplement (1988). The LRS was a slitless spectrometer with two wavelength channels recording from 7.7 to 13.4 μm and from 11.0 to 22.7 μm, respectively. In each band, the wavelength resolution varies between 10 and 60. The LRS wavelength range thus includes the 7.7 μm emission feature (at least, the long wavelength side of the emission band), the 8.6 μm feature which may or may not appear as a shoulder on the long-wavelength wing of the 7.7 μm band, and the 11.3 μm emission band with, longward of it, the "plateau emission" extending out to $\sim$ 13 μm.

The IRAS/LRS data base contains a few hundred sources characterized by a red spectrum (rising with wavelength) which are associated with HII regions, reflection nebulae, planetary and proto-planetary nebulae, young embedded objects and a few galaxies. In a recent study, Jourdain de Muizon et al. (1990a) showed that the 7.7, 8.6 and 11.3 μm emission features are *ubiquitous* in the spectra of HII regions, reflection nebulae and, for C/O ratio greater than one, in planetary nebulae. This data base of about three hundred sources was presented in a qualitative study, emphasizing the description of the spectra (presence or not of atomic, molecular or dust features and bands) and the statistics of the sample. LRS spectra of bright IRAS sources have also been published by Volk and Cohen (1989a, 1990).

Our primary selection was based on the study by Jourdain de Muizon et al. (1990a) and the publications by Volk and Cohen (1989a, 1990). Additional sources were extracted from the IRAS/LRS data base by searching for HII regions identified in the 5 GHz radio surveys of Effelsberg (Wink et al., 1982) and Parkes (Haynes et al., 1978), and for sources located in the outer solar circle in the catalogue of Wouterloot and Brand (1989). To minimize corrections due to extinction, we rejected from the primary selection sources *clearly* showing in their spectra the silicate absorption features (at 9.7 and/or 18 μm). This resulted in a rejection of about hundred sources. The extinction effect was considered negligible for the remaining sources since no correction for interstellar extinction is made in this study.

The fact that the LRS was a slitless spectrometer renders the derivation of line fluxes somewhat difficult and, as stressed in Jourdain de Muizon et al. (1990a), " considerable care has to be taken to carry out any quantitative investigation of the LRS spectra ". Therefore, great attention has been given to the quality of the data, namely : presence of spurious spikes (see Muizon et al., 1988), and a close examination of the individual spectra.

The final sample contains 113 sources and includes 77 HII regions, 25 reflection nebulae, 7 planetary nebulae and 4 galaxies.

2.2. Derivation of the band strengths

We checked the consistency between the color-corrected 12 μm flux density from the IRAS Point Source Catalog (2^d version) and the integrated flux in the LRS spectra after multiplication with the survey pass-band. In general, the IRAS spectra and the photometric data agree to within 10 - 15% (see IRAS Explanatory Supplement IX-9), but in some cases we found significant discrepancies. For those spectra, we applied a linear correction factor to the spectral data in order to be consistent with the photometric data. The reason for these calibration discrepancies remains, however, unclear to us (see Volk and Cohen, 1989b for a detailed discussion on the IRAS/LRS calibration problem). The resulting uncertainties, however, are considered not to affect significantly the PAHs band strengths but could increase the error in the continuum estimate. No correction was applied for the few sources in our sample with 12 μm flux densities of bad quality with (:) or (L) flags in the IRAS/PSC and labeled with an asterisk in Table 1.

The intensities of the PAH emission bands were measured by subtracting the integrated strengths of the features from the underlying continuum in the intervals 7.5 to 10 μm for the 7.7 and 8.6 μm bands (Band I) and 11 to 12 μm for the 11.3 μm band (Band II). For Band I, we assumed that the continuum is constant over the wavelength range from 7.5 μm to about 10 μm; the level of the continuum was taken to be the intensity measured around 10 μm by the LRS which is the part of the spectrum uncontaminated by PAH emission. Since the LRS did not cover the 7.3 to 7.6 μm spectral range, the short wavelength part of the 7.7 μm band, the strength of Band I is thus underestimated. Comparing with published KAO spectra covering the entire 7.7 μm emission feature (Cohen et al., 1986, 1989), we estimate that the flux contained between 7.3 and 7.6 μm only represents a small fraction (less than 20%) of the total 7.7 μm band flux. Since this contribution is small compared to the LRS noise level as defined below, we did not apply any correction. The low wavelength resolution of the LRS does not allow one to separate the generally

weak 8.6 μm emission band from the intense 7.7 μm band. Even from the high quality (both in spectral resolution and coverage) spectrum of the Orion Bar published by Bregman et al. (1989), it is difficult to determine exactly the relative strengths of the 7.7 and 8.6 μm bands. Therefore, we decided to include in our estimates of the 7.7 μm band strength the contribution of the 8.6 μm emission feature. We made, for some spectra, several measurements with different choices for the continuum definition, in order to estimate the uncertainty on the intensity measurement in Band I. In the worst cases, uncertainties up to 25% were found. On the average, the uncertainty is less than 20%.

The strength of the 11.3 μm emission feature has been measured by defining a local uniform continuum interpolated between spectral regions around 10 μm and 13.5 μm where no line or feature contamination is expected. The continuum was defined so as to be compatible with the spectral data at wavelengths longer than 13.5 μm recorded by the long wavelength channel of the LRS. The relative uncertainty on the 11.3 μm band flux is estimated to be about 20% applying the same procedure as for Band I. In addition to the 11.3 μm feature, a broader emission band is often present which extends to about 13 μm. This "plateau emission" is best traced in sources with a strong 11.3 μm emission band and is commonly attributed to the CH out-of-plane bending mode of PAHs with different degrees of hydrogenation (Allamandola et al., 1989). We did not try to include the strength of this broad structure in the estimate of the 11.3 μm feature strength, since it is difficult to separate it from the underlying continuum. The "plateau emission" is thus part of the mid-infrared continuum. In the best observational case, the Orion Bar (Geballe et al., 1989), the plateau emission strength does not exceed 40 % of the 11.3 μm feature strength. Note that the choice of the integration limits for the 11.3 μm feature (from 11 to 12 μm) also excludes the 12.8 μm [NeII] line present in most of the spectra.

Figure 1 shows the IRAS/LRS spectra of eight typical sources, chosen in order to illustrate the various kinds of spectra encountered in this study. Also shown for one of the sources is the adopted continuum.

Compared with the results by Jourdain de Muizon et al. (1990b), we derive systematically higher values for the intensities of the (7.7 + 8.6) μm bands. The discrepancies probably originate from the different integration limits used to estimate the (7.7 + 8.6) μm band strengths. For the 11.3 μm emission band, the main cause of the small discrepancy between the study of Jourdain de Muizon et al. and this work resides in the choice of the continuum. The differences are normally less than 30% except in two cases (IRAS 18184−1302 and IRAS 18416−0420) where there is a 50% difference.

The results are presented in Table 1 for the 113 sources of the final sample together with some of their physical properties. The Table has four sections corresponding to the HII regions, the reflection nebulae, the planetary nebulae and the galaxies. An extra section presents for comparison two standard sources: the Orion Bar and the planetary nebula NGC 7207. Columns 1 and 2 give the IRAS name of the source and the association when available. The measured intensity of the (7.7 + 8.6) μm features, Band I, and 11.3 μm feature, Band II, are listed in column 3 and 4. Column 5 displays the "LRS1" Band which gives the total flux integrated from 7.5 to 13.5 μm recorded by the short wavelength channel of the LRS. This band contains therefore all three PAH emission bands (7.7, 8.6 and 11.3 μm) without sampling the continuum at longer wavelengths as does the IRAS

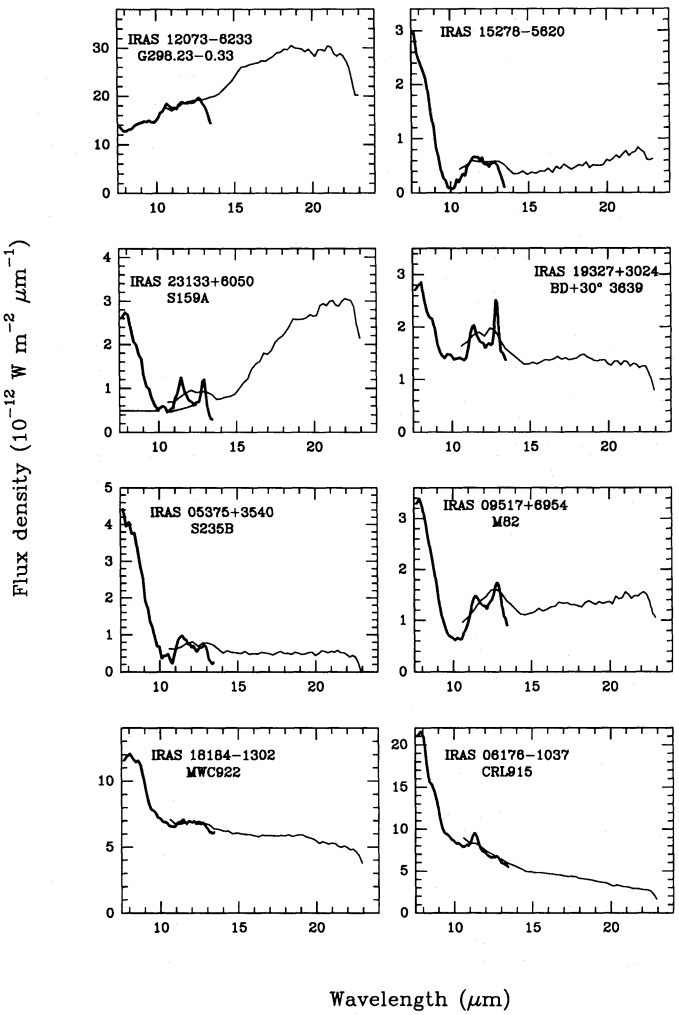

Fig. 1. Typical spectra from the sample selected for this study. IRAS 12073-6233: HII region strongly dominated by the underlying continuum; the 7.7 μm feature is not clearly seen. IRAS 23133+6050: HII region showing the emission features above the underlying continuum, with strong emission at wavelengths longer than 15 μm. The adopted continuum (see the text) is shown. IRAS 05375+3540: HII region showing strong emission features with a flat spectrum at long wavelengths. IRAS 18184-1302: Reflection nebula dominated by the underlying continuum and showing the emission features. IRAS 15278-5620: Reflection nebula dominated by the emission features. IRAS 19327+3024: The well-known planetary nebula BD+30°3639 showing the emission features above the strong underlying continuum. IRAS 09517+5954: Spectrum of the galaxy M82; the emission features are clearly seen. IRAS 06176-1037: Spectrum of the planetary nebula CRL 915; note the smooth decreasing part at wavelengths longer than 15 μm.

12 μm band which extends from 7.7 to 14.5 μm. We will refer to "LRS1" to evaluate the contribution of the PAH emission features to the mid-infrared fluxes. Columns 6 to 9 tabulate the following physical parameters: the distance to the Sun ($D_\odot$), the distance to the Galactic Center (R_G), the number of Lyman continuum photons (N_{Lyc}) and the infrared luminosity (L_{IR}). References to the literature are given in Column 10.

Table 1. Properties of the IRAS/LRS Sources

IRAS Name	Association	$F_{(7.7+8.6\,\mu m)}$	$F_{(11.3\,\mu m)}$	LRS1	D_{sun}	R_G	N_{Lyc}	$L/L_\odot$	Ref.
		(10^{-18} W.cm^{-2})			(kpc)		(s^{-1})		
		HII Regions							
01056+6251	G124.90+0.33,S186	74	15	175	3.1	10.5	1.5(47)	5.1(3)	FH
02575+6017	IC1848,AFGL4029	138	15	403	3.8	11.7		4.0(4)	WB
02593+6016	S201,AFGL416	159	13	360	3.9	11.7		5.6(4)	WB
03035+5819	AFGL437,BFS26	173	22	813	4.1	11.9		6.7(4)	WB
04324+5106	AFGL5124	82	23	182	5.8	14.0		6.4(4)	WB
05375+3540	S235B	626	54	846	1.6	11.6	7.7(46)	1.3(4)	
05393–0156	NGC2024	5480	443	7300	0.5		1.0(48)	1.6(4)	
06073+1249	AFGL5185,S270	80	15	164	5.9	14.3		5.7(4)	WB
06117+1350	S269	175	14	294	3.8	12.2		6.0(4)	WB
08189-3602	G254.68+0.23,PK254+0.1	174	17	750	6.0	11.6	1.2(49)	1.8(5)	CH
08546-4254	G264.29+1.48,RCW34	216	16	507	2.0	8.9	9.9(47)	1.5(4)	CH
08563–4711	VHE26	259	38	556	1.7	8.7		2.5(4)	WB
09002–4732	G268.45-0.85	1020	121	2660	1.5	8.7	7.1(47)	6.9(4)	CH
09149–4743	G270.39+0.85	167	21	303	2.7	8.9	4.2(48)	2.5(4)	CH
09563–5743	G281.56-2.48	132	20	204	5.0*	9.0*	1.4(48)	7.7(4)	HCS
10031–5632	G281.60-0.97	147	28	279	3.7	8.6	1.1(48)	4.2(4)	CH
10320–5928	G286.40-1.35	98	13	320	8.3	10.1	9.6(48)	2.0(5)	CH
10589–6034	G289.88-0.79	272	33	603	7.8	9.4	2.0(49)	2.8(5)	CH
11143–6113	G291.86-0.68			359	8.5	9.5	2.0(49)	1.4(5)	CH
12063–6259	G298.19-0.78,He2-77	270	48	644	9.3	9.2	1.8(49)	4.5(5)	CH
12073–6233	G298.23-0.33			9760	10.5	9.9	2.2(50)	4.1(6)	CH
12331–6134	G301.11+0.97	293	27	730	4.4	7.3	6.5(48)	8.7(4)	CH
12437–6218		77	8	101					
13291–6229	G307.62	543	56	810	2.9*	7.2	5.8(48)		CH
13291–6249	G307.57-0.62	111	37	248	2.7*	7.1	7.1(47)	2.5(4)	CH
14382–6017	G316.16-0.49	271	32	388	3.8*	6.3	1.7(48)	6.5(4)	CH
14453–5912	G317.40+0.11	225	32	407	3.1*	6.5*	7.4(47)	3.3(4)	HCS
14593–5852	G319.16-0.42	175	28	274	11.6	7.6	5.1(49)	5.3(5)	CH
14594–5824	G319.38-0.03	278	52	530	12.1	7.9	6.3(49)	1.1(6)	CH
15384–5348	G326.44+0.91	760	64	1310	2.4	6.6	4.0(48)	8.1(4)	CH
15408–5356	G326.65+0.59,RCW95 *	1060	110	4121	2.6	6.5	1.5(49)	1.9(5)	CH
15530–5231	G328.94+0.55	213	33	280	7.2	4.5	3.3(48)	1.6(5)	HCS
15544–5159		87	13	207					
15557–5337	G328.59-0.52,RCW99 *	984	109	5670	3.1	6.0	7.2(48)	2.5(5)	CH
16026–5035	G331.35+1.07 *	657	92	1810	4.9*	4.8	1.2(49)		CH
16085–5138	G331.31-0.34 *			1310	4.0	5.4	1.2(49)	1.0(5)	CH
16128–5109	G332.15-0.45	888	60	1900	3.4	5.7	1.2(49)	1.9(5)	CH
16156–5002	G333.24+0.05	357	20	762					
16164–4929	G333.72+0.36	211	28	393	2.5*	6.4*	2.5(47)	2.5(4)	HCS
16313–4840		188	24	349					
16362–4845	G336.51-1.48,RCW108	999	162	2680	1.8	6.9	1.9(48)	1.2(5)	CH
16374–4701	G337.95-0.48 *			1970	2.9	6.0	1.1(49)	3.1(5)	CH
16396–4429		267	33	421					
16571–4029	G345.23+1.04 *	1610	113	4040	1.0	7.6	9.1(47)	2.2(4)	CH
17059–4132	G345.43-0.94, H2-3 *			13700	2.4	6.2	1.6(49)	2.7(5)	CH
17149–3916	G348.23-0.98, H2-6 *			6050	2.3	6.3	6.3(48)	9.4(4)	CH
17199–3445		147	11	279					
17271–3439	G353.43-0.37	500	77	930	3.2*	5.3	8.1(48)	1.8(5)	CH
17279–3350	G354.20-0.05	121	13	367	5.5*	3.1	1.4(49)	1.3(5)	CH
17439–2845	S20	298	37	514					
17545–2357	G5.632	102	14	167					
18032–2032	G9.61+0.20	349	51	594	0.5*	8.0	3.8(46)	2.5(3)	WAM
18116–1646	G13.88+0.28	574	62	990	4.6*	4.2	7.3(48)	2.2(5)	WAM
18162–1612	AFGL2121	124	21	168					
18295–1030	G21.42-0.57	233	25	287	5.5*	3.4*	1.5(48)	5.5(4)	R84
18317–0757	G23.96+0.15	404	30	958	5.1*	4.3	4.9(48)	1.7(5)	WAM
18379–0500	G27.28+0.15 *	88	22	196	12.9*	6.6	1.3(49)	2.6(5)	WWB
18416–0420	G28.29-0.37	474	65	1270	2.2*	6.6	3.8(47)	4.8(4)	WAM
18469–0132	G31.40-0.26 *	190	36	569	5.7	4.7	1.9(48)	1.5(5)	WWB
18502+0051	G33.91+0.11	127	18	378	7.0	4.8	7.0(48)	2.0(5)	WAM
18530+0215	G35.46+0.14	152	18	305	3.0*	6.3*	3.7(47)	3.2(4)	A78
19097+0847	G43-0.52	160	18	242	3.9	6.3	8.0(47)	3.3(4)	WAM
19120+0917	GG43.89-0.79	121	10	195	8.8	6.5	5.3(48)	1.8(5)	W88
19205+1403	G49.076	132	20	392	6.6	7.6	4.2(48)		

Table 1. (continued)

IRAS Name	Association	$F_{(7.7+8.6\,\mu m)}$	$F_{(11.3\,\mu m)}$	LRS1	D_{sun}	R_G	N_{Lyc}	$L/L_\odot$	Ref.
		(10^{-18} W.cm^{-2})			(kpc)		(s^{-1})		
HII Regions (continued)									
19213+1723	G52.10+1.04	157	26	297	4.3*	6.8*	9.9(47)	2.7(4)	WAM
19442+2427	S87	630	34	1010	2.3	9.1	3.5(47)		
19446+2505	S88B *	1240	97	3480	2.5	9.2	2.1(48)	9.1(4)	
20375+4109	DR22	763	60	1260	3.4	10.0			
21190+5140	G93.53+1.47,M1-78	98	22	462	6.8	11.2	4.9(48)	1.3(5)	P88
22308+5813	G105.63-0.34,S138	199	34	481	4.5	10.6	1.2(48)	4.9(4)	F86
22475+5939	G108.19+0.58,S146	134	26	365	5.1	11.	5.9(48)	6.0(4)	FH
22542+5815	AFGL2991,S148	172	12	261	5.5	11.5		4.8(4)	WB
22551+6221	S155	229	26	490	1.5	9.1		1.2(4)	WB
23030+5958	G110.11+0.05,S156	286	37	578	3.5	10.2	3.1(48)	5.0(4)	I77
23133+6050	G11.62+0.37,S159A	325	40	760	3.5	10.3	1.7(48)	7.8(4)	B78
23138+5945	AFGL3057,S157A	294	24	542	4.5	10.9	1.1(48)	1.0(5)	WB
23152+6034	MWC1080	66	8	330	2.2		1.8(47)	6.3(3)	AC89
Reflection Nebulae									
03211+5446	AFGL594,BFS31	160	12	241	3.4	11.4		1.8(4)	WB
03260+3111	AFGL5096	350	79	753					
05044-0325	CED40	152	20	218					
05391-0217	NGC2023	352	41	602	0.5			1.1(3)	
06063+2040	AFGL5183 *	325	19	917	2.8	11.3		2.8(4)	WB
06114+1745	AFGL5188	155	17	287	1.7	10.1		4.3(3)	WB
06158+1517		85	15	168	9.4	17.7		6.4(4)	WB
06572-0742	Parsamyan18	133	20	335	1.2	9.4		2.1(3)	WB
08470-4243	BBW186	134	11	278	2.2	9.1		1.6(4)	WB
08513-4201	DC263.2+1.6	126	26	159					
09014-4736	BBW225	243	18	559	1.3	8.6		3.7(3)	WB
10591-5934	G289.52 *	252	22	847					
11332-6258	G294.5-0.16	64	8	125					
12389-6147		205	21	775					
15246-5612	G323.44	187	14	219					
15278-5620		374	31	673	3.0				
16555-4237	CD-42°11721	852	139	1780					
18184-1302	MCW922	899	62	4830					
19343+2026	*	195	22	407					
20293+3952		156	19	387	1.0			9.0(3)	
20319+3958		260	31	492					
21009+6758	NGC7023	273	33	416	0.44				
21202+5157		80	13	140	7.7	11.8		8.0(4)	WB
22539+5758		64	13	113	3.5			1.2(4)	WB
23042+6000	BFS18	118	14	260	5.5	11.6		5.5(4)	WB
Proto-Planetary and Planetary Nebulae									
06176-1037	CRL915	2180	155	6110					
07027-7934		95	10	352					
14562-5406	He-113	277	23	1340					
17047-5650	CP-56°8032	802	41	2350					
18240-0244	M2-42	62	15	193					
19327+3024	BD+30°3639	176	43	1090	2.8				M
21282+5050		112	49	547					
Galaxies									
00450-2533	NGC253	136	40.1	276	4170			3.1(10)	R
09517+6954	M82	331	63.5	894	3500			2.3(10)	R
13025-4911	NGC4945	43	7	58	6920			5.5(10)	R
13225-4245	NGC5128, CentA	116	32	170	6920			2.0(10)	R
Standard Sources									
	Orion Bar	38	9		0.46				R89
	NGC 7027	798	297	4731	0.9				R77

Alonso-Costa et al., 1989 (AC89); Altenhoff et al., 1978 (A78); Birkinshaw, 1978 (B78); Caswell and Haynes, 1987 (CH); Felli and Harten, 1981 (FH); Fich, 1986 (F86); Haynes et al., 1979 (HCS); Israel, 1977 (I77); Masson, 1989 (M); Puche et al., 1988 (P88); Sellgren et al., 1985 (S85); Reich et al., 1984 (R84); Rice et al., 1989 (R89); Roche, 1989 (R89); Russell et al., ,1977 (R77); Wink et al., 1982 (WAM); Wink et al., 1983 (WWB); Wood et al., 1988 (W88); Wouterloot and Brand, 1989 (WB).

Note to Table 1: (*) the 12 μm is of poor quality.

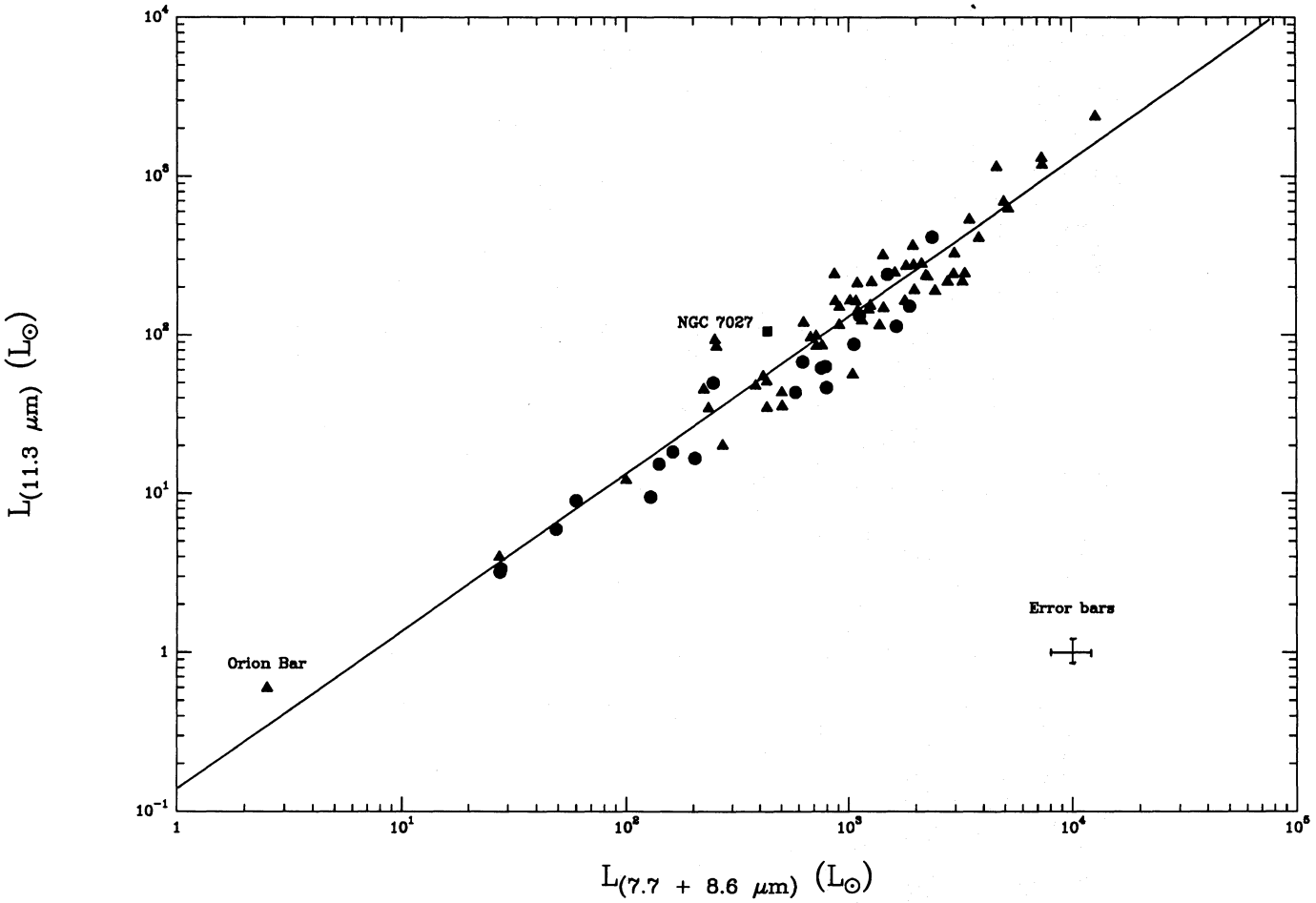

Fig. 2. Correlation between the luminosities of the sum of the 7.7 and 8.6 μm emission bands and the 11.3 μm emission band for the galactic sample of 77 sources given in Table 1 for which distances are known. HII regions are shown by filled triangles, reflection nebulae by filled circles, planetary nebulae by filled squares. The band luminosities of the well-known sources NGC 7027 and the Orion Bar are also shown. The straight line represent the least-squared fit given in the text.

3. Results

Figure 2 compares the luminosity of the 11.3 μm emission band $L_{11.3\,\mu m}$ with the sum of the luminosities of the 7.7 and 8.6 μm emission bands $L_{(7.7+8.6\,\mu m)}$ for the galactic sample. The observed strengths were converted into luminosities taking the distance given in Table 1 (known for 77 sources). The different types of sources (HII regions, reflection nebulae, and planetary nebulae) are displayed with different symbols. The mean errors are shown (20% for Bands I and II). Also displayed and labelled in Fig. 2 are the Orion Bar and the planetary nebula NGC 7027.

A definite correlation is seen in Fig. 2. We have fitted a straight line to all the data points in Fig. 2 by least-squared techniques:

$\log_{10} L_{11.3\,\mu m} = a \log_{10} L_{(7.7+8.6\,\mu m)} + b$

For the galactic sources, we find the following coefficients:

$a = 1.003 \pm 0.034$ and $b = -0.919 \pm 0.165$

with a correlation coefficient r^2 of 0.92 .

The value of the slope is nearly equal to unity indicating that the luminosities of the emission features are linearly correlated. These findings significantly extend the results published by Cohen et al. (1986, 1989). These authors derived for a sample of 22 sources a linear correlation between both PAH emission bands at 7.7 and 11.3 μm with the coefficients $a = 0.92 \pm 0.21$ and $b = -0.44 \pm 0.26$ and a correlation coefficient of $r^2 = 0.82$, in accordance with the present results.

It is truly remarkable that *all* the sources follow the same correlation (despite the differences in physical conditions) and that the dispersion remains so small (30%, i.e. of the order of the estimated error for the ratio of measured bands strengths), over such a wide range of luminosities (four decades for the galactic sample). The histogram of the distribution of the ratio $F(7.7 + 8.6\,\mu m)/F(11.3\,\mu m)$ is displayed in Fig. 3 illustrating, for the complete sample (the six sources with no PAH band strength measurement excepted), the distribution of this ratio around the mean value of $8.3^{+3.8}_{-2.6}$. The scatter remains within the error bars of the intensity measurements for each band.

Figure 4 presents the histograms of the contribution of the emission bands (sum of the 7.7, 8.6 and 11.3 μm fluxes) to the flux measured in the LRS1 Band, i.e. F(PAH Bands)/F(LRS1), for each type of sources (HII regions, reflection nebulae, planetary nebulae and galaxies). From Fig. 4, it can be seen that the contribution of the emission bands to the LRS1 band strength varies over a large range from 15% to 100%. For six HII regions, the underlying continuum is so strong that it is impossible with the present spectral data to measure the strength of the emission

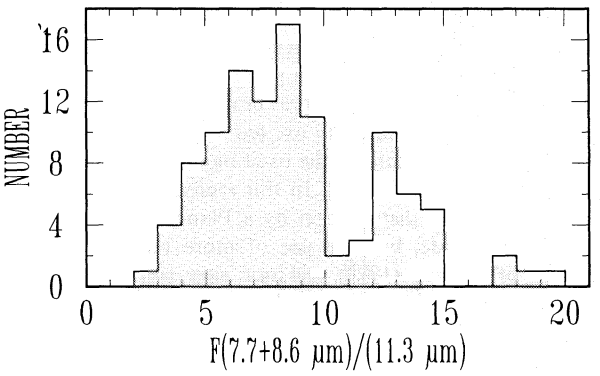

Fig. 3. Histogram of F(7.7+8.6 μm)/F(11.3 μm) for the sample of Table 1.

features. We conclude that, for these sources, the contribution is less than 5%. With the selection criteria used for this study, in section 2, these are the only sources which do not exhibit clearly the emission features above the underlying continuum. In fact, the upper limit for the band strength, as provided from their estimated contribution, is still compatible with the trend found in this study. These sources are not used, however, in establishing the correlation found in Fig. 2. The distribution for the statistically most significant sample of HII regions peaks in the range 40 - 70% . The sample of reflection nebulae has a quite similar distribution than for the HII regions. The mean value for the smaller sample of planetary nebulae is less with a value of about 30%, indicating that the continuum dominates in these sources. It is interesting to note that the mean value of 50 - 60 % is comparable to the value observed for the galaxies.

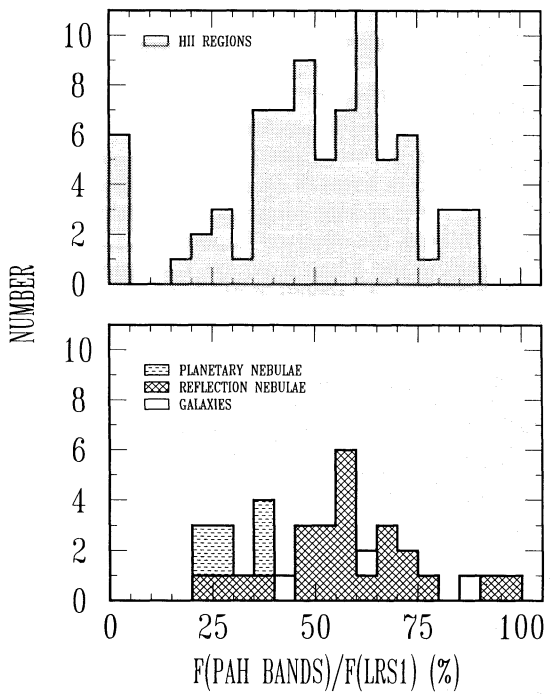

Fig. 4. Histograms of the distribution of F(PAH Bands)/F(LRS1) i.e the contribution (in percent) of the emission bands at 7.7, 8.6 and 11.3 μm to the total flux measured between 7.5 and 13.5 μm (the LRS1 Band) for the different types of sources discussed in the text.

To study the influence of the excitation conditions on the contribution of emission features to the LRS1 band, we have computed the ratio F(PAH Bands)/F(LRS1) for two sub-samples of HII regions: first for the 26 HII regions with a number of Lyman continuum photons (N_{Lyc}) smaller than 3×10^{48} ph s^{-1} (corresponding to a O7.5 ZAMS exciting star, Panagia 1973), second for the 32 HII regions with N_{Lyc} greater than 3×10^{48} ph s^{-1}. No significant difference has been found between the two sub-samples: for $N_{Lyc} \leq 3 \times 10^{48}$ ph s^{-1}, F(PAH Bands)/F(LRS1) is greater than 50% for two third of the sources, whereas for $N_{Lyc} \geq 3 \times 10^{48}$ ph s^{-1} F(PAH Bands)/F(LRS1) is less than 45% for half of the sources. However, we note that the HII regions dominated by the continuum (and not the emission bands) are highly excited sources.

4. Discussion

4.1. Preliminary considerations

From the characteristics of the LRS, the sample under consideration is biased towards isolated, compact sources with typical sizes of about 30 arcsec or smaller. This fact together with the large beam of IRAS (a few arcmin) limits this study to the analysis of global characteristics. In particular, the physical properties of the sources presented in Table 1 are derived from single dish radio measurements taken with beams comparable to the IRAS beam. The listed properties are thus averaged over the source geometry, the density structure and the distribution of the ionized/neutral gas. Detailed spatial studies are excluded by the present data and only systematic studies such as statistical analysis or global energetical budgets are possible. These limitations are however compensated by the homogeneity of the IRAS/LRS data set and the great number of sources contained in the data base. A study on the abundance distribution in the Galaxy, based on the LRS data and with comparable bias and limitations has been presented by Simpson and Rubin (1990).

The scope of the following discussion is to constrain the properties of the molecular species responsible for the emission bands and, if possible, of the carriers of the underlying continuum on the basis of the relations and trends presented in Section III.

4.2. Correlation between the band strengths

The facts that the correlation between the luminosities of the 7.7 and 11.3 μm emission bands (Fig. 2) follows a slope nearly equal to unity and that the spread around the mean value of 8.3 is as small as 30% confirm that the carriers of both features belong to the *same* family. This result should be compared with the study of the 7.7 and 6.2 μm band intensities based on KAO measurements by Cohen et al. (1989). For these emission bands a correlation coefficient of unity was found for a sample of 40 sources (Cohen et al., 1989). An equivalent result is thus expected from the comparison of the 6.2 and 11.3 μm emission bands. However, we decided not to include this comparison to avoid using inhomogeneous data bases. For the same reason, we did not compare the LRS data with published data on the 3.3 μm. A complete homogeneous study of the near and mid-infrared emission features is likely to be one of the outcomes of the forthcoming ISO mission.

Such relations imply a similar type of carrier for *all* the mid-infrared emission bands. The most commonly accepted carriers are polycyclic aromatic hydrocarbons or PAHs (Puget and Léger,

1989; Allamandola et al., 1989), although other generic families such as HACs (Duley and Williams, 1981) or QCCs (Sakata et al., 1984) have been proposed. However, no specific molecule (or type of molecule) has yet been found which reproduces all the characteristics of the astrophysical near and mid-infrared spectra.

The above results might further constraint the physical characterisitics of the carriers. The ratio of the 7.7 and 11.3 μm emission bands which are related to the C $\equiv$ C and C-H bending modes of the aromatic species, is measured to yield an average value of about 8. Proposed carriers should obviously reproduce this value. It is interesting to note that recent theoretical calculations by de Frees et al. (1992) and Ellinger et al. (in preparation) on small aromatic compounds (naphtalene, anthracene and pyrene) show that a ratio of about 10 between the intensities of the 7.7 and 11.3 μm is typical for ionized species (neutral species have an intensity ratio of about 0.3). The ratio found in the present study might thus suggest that the aromatic compounds are ionized in the neighbourhood of HII regions, reflection nebulae and planetary nebulae. Although such a conclusion appears consistent with the facts that, first, the sources under study are characterized by strong radiation fields and second, that the ionization potential of PAHs is low (around 7-8 eV), further studies on larger compounds (such as coronene) and a comparison with laboratory data should be done before any firmer conclusion can be reached.

The relatively small dispersion in the value of the bands ratio is certainly another constraint for any candidate. Although lying within the intrinsic measurement errors, part of the variation is most likely due to the large range of physical conditions of the present sample. Probable causes are: variations in the flux of the exciting photons, different C/H ratios of the molecular carriers or variations in the sizes (hence in the emission temperatures). To further study these differences, data with higher sensitivity, better spectral resolution and wavelength coverage are clearly needed.

4.3. Excitation of the emission bands

The basic excitation mechanism of PAHs and related species is considered to be absorption of UV photons. However, it has been recognised that visual photons could excite, as well as UV ones, the emission bands from very small particules in the mid-infrared (Allamandolla et al., 1989, Léger et al., 1989, and Sellgren et al., 1990).

A quantitative analysis of the excitation of the emission features at 7.7, 8.6 and 11.3 μm can be done with the present data for the HII regions. Figure 6 shows the dependence of the luminosity contained in the emission features (refered to as L_{PAH}) upon the number of Lyman continuum photons (N_{Lyc}) as given in Table 1. In Fig. 5, the straight line with slope unity (labeled "100% L_{Lyc}") shows the relation for a 100% conversion efficiency of the photons with energies $h\nu > 13.6$ eV into the three emission bands.

For low values of N_{Lyc}, the luminosity of the emission bands is close, for certain sources, to the total available luminosity in the Lyman continuum. This behaviour shows that the Lyman continuum photons cannot provide the main contribution of the excitation of the PAH emission bands observed at 7.7 and 11.3 μm. In the case of the 7.7μm band, only an upper limit of 1.2% of the available luminosity in the Lyman continuum is expected to be converted in the 7.7μm band luminosity, derived from a simple energy ratio. Since L_{PAH} also includes the bands at 8.6 and 11.3μm, this upper limit could be increased up to 2.5% at maximum. This is in evident contradiction with the fact stated above that L_{PAH} is close in certain cases to L_{Lyc}. UV and visible photons, less energetic than Lyman continuum ones, are thus necessary to provide the required luminosity.

Assuming that each source is excited by a single star, the range of effective temperature of the exciting star can be derived from N_{Lyc} (see e.g. Panagia, 1973). In this study, we will approximate the stellar energy distribution by a Planck function. This is a first order estimate, but the use of more realistic models such as those of Kurucz (1979) will not alter significantly the conclusions found in this paper. Under these assumptions, the energetic contribution of any wavelength range can be computed for $\lambda \geq 91.2$ nm. Arbitrarily, we have considered the following domains from the UV to the visible: 91-182 nm, 182-365 nm, and 365-730 nm. For each domain, the maximum available luminosity, allowed within the effective temperature range derived from N_{Lyc}, is computed. Taking into account the differences in energy between photons in the above selected ranges and in the PAH emission bands at 7.7 and 11.3 μm, conversion efficiencies of 5%, 10% and 20% are expected in each of the wavelength ranges defined above. The curves (approximately straight lines) corresponding to the highest luminosity (lowest acceptable temperature for a given N_{Lyc}) available, for each spectral range, are presented in Fig.5. The curve labelled "0-91.2 nm" corresponds to the 2.5% maximum conversion efficiency of the Lyman continuum luminosity.

From Fig. 5, one can see that none of the spectral ranges considered can provide, by itself, the energy needed to yield the luminosity of the 7.7 and 11.3 μm observed from the sources under investigation. The slope of the luminosity available in the wavelength range 182 - 365 nm match rather well the data points. However, the values of L_{PAH} imply clearly that absorption is needed over the whole UV range to provide the required excitation of the emission bands. As shown by laboratory measurements, the absorption of PAH species is the most efficient in the ultraviolet domain (Léger et al., 1989, Allamandola et al., 1989, Verstraete et al., 1990).

The overall efficiency of the photon conversion, as derived from the present analysis, seems to be extremely high, at least for part of the sources. Note, in this respect, that the 7.7μm band is the most constraining one in terms of energy conversion, i.e. each UV photon absorbed in the specific ranges needs to be converted in a 7.7μm photon. Indeed, the observed luminosity ratios of the 3.3, 6.2, 11.3 μm bands to the 7.7μm band are, respectively, 0.01-0.2 (Jourdain de Muizon et al., 1990b), 0.54 (Cohen et al., 1989) and 0.120 (this work), instead of 2.33, 1.24 and 0.68, as expected from simple energetic consideration only.

4.4. Energetics and abundance estimates

4.4.1. Emission bands

The fraction of elemental carbon locked in the carriers of the 7.7 and 11.3 μm emission bands (f_C) can be derived from their contribution (f_{ir}) to the total infrared dust continuum. The following estimates are given for PAH molecules. From Allamandola et al. (1989), the fraction of carbon in the form of PAH molecules is given by

$$f_C = \frac{1.6 \times 10^{-18}}{\sigma_{uv}} \frac{f_{ir}}{(1-f_{ir})}$$

where $f_{ir} = F_{PAH}/F_{IR}$. F_{PAH} represents the flux contained in the emission bands, F_{IR} is the infrared dust continuum flux approximated by the sum $\sum \nu_i F_{\nu_i}$ over the four IRAS bands,

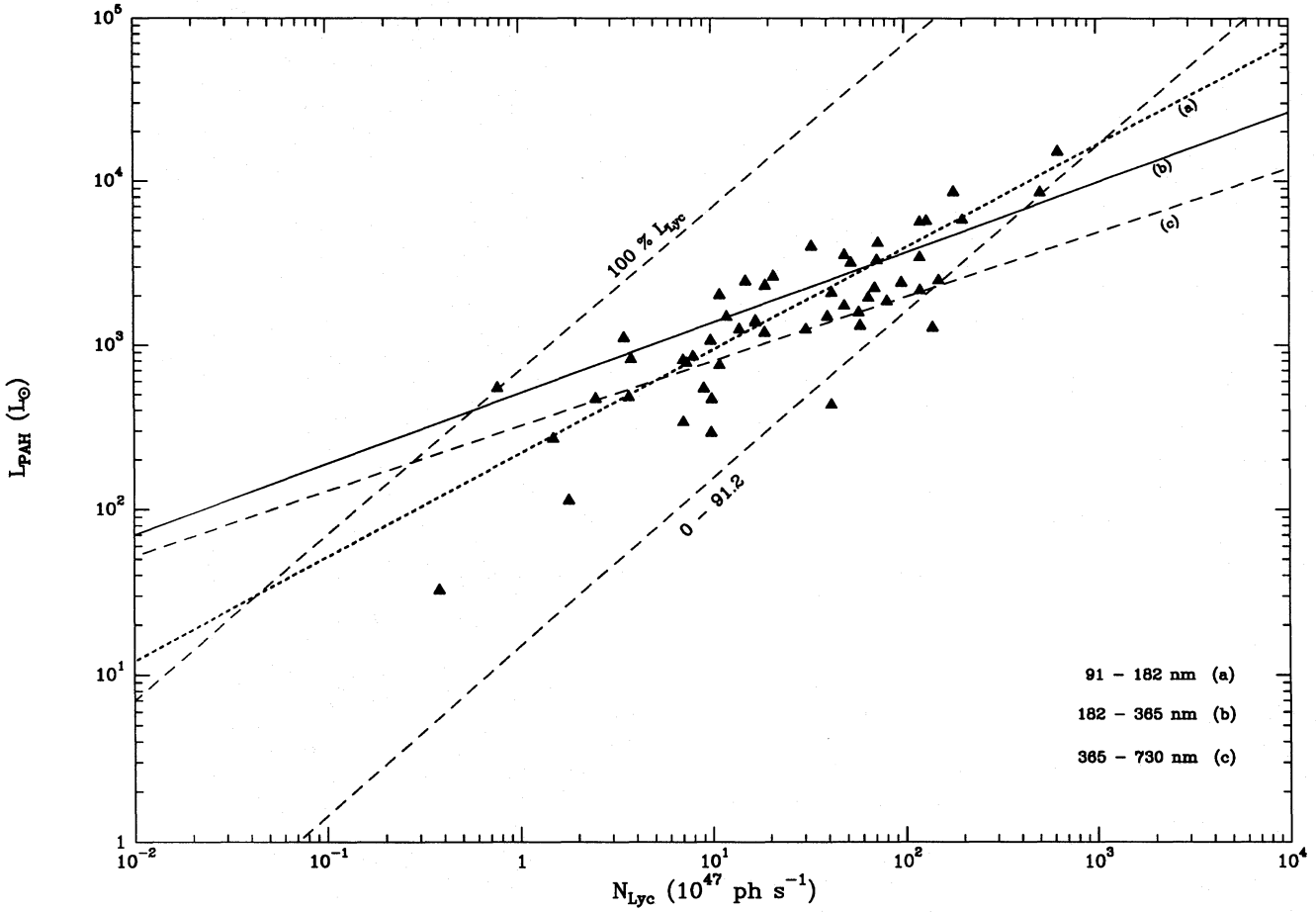

Fig. 5. Luminosity contained in the emission bands at 7.7, 8.6 and 11.3 μm (refered to as L_{PAH}) as a function of the number of Lyman continuum photons (N_{Lyc}) for 51 HII regions. The curves labelled (a), (b) and (c) show the highest possible luminosity available for the spectral ranges given in the Figure, whereas the dotted line labeled "0 - 91.2" corresponds to the Lyman continuum domain (see text). The dotted line labeled "100% L_{Lyc}" corresponds to a 100% conversion efficiency of photons with $h\nu > 13.6$ eV into the three emission bands.

σ_{uv} is the average UV absorption cross section of PAH per carbon atom and the numerical coefficient has been estimated for standard values of the dust and gas properties (using an elemental carbon abundance C/H = 4×10^{-4}).

The absorption properties of PAH molecules are characterized by a strong absorption peak in the 200 - 250 nm range followed by a continuum rise in the far-UV range, peaking at about 70 nm (see e.g. Verstaete, 1990). The absorption cross sections, however, vary from species to species, and since the identification of the species responsible for the observed spectra is still unknown, the choice is somewhat arbitrary. For species such as coronene, the average cross section values in the range 91 - 300 nm are large, typically 2×10^{-17} cm^2 per carbon atom, whereas for larger species or mixtures the values are on the order of a few 10^{-18} cm^2. We will adopt a value of 3×10^{-18} cm^2 per carbon atom to estimate f_C.

From the present data f_{ir} (and hence f_C) will be underestimated since the LRS spectra did not measure the strong 6.2 μm emission feature. Cohen et al. (1989) have derived for the ratio I(6.2 μm)/I(7.7 μm) a mean value of 0.54, implying that f_{ir} is about 40% higher than the estimate based on the 11.3, 8.6 and 7.7 μm emission features alone. Given the uncertainties in deriving f_{ir}, the contribution of the 3.3 μm band was considered not to be significant, and hence not taken into account. Considering the numbers for the galaxies in our sample as representative, we estimate, for M82, $f_{ir} \sim 4\%$ after correcting for the 6.2 μm band contribution. This value, based on the LRS spectrum, is in agreement with estimates made by Puget and Léger (1989) and Allamandola et al. (1989) derived from the complete KAO/ground-based spectrum of Willner et al. (1977).

The histogram of the distribution of f_{ir}, as derived from the 7.7, 8.6 and 11.3 μm emission band fluxes and the infrared dust continuum flux is shown in the upper panel of Fig. 6 for the sample of Table 1 (excluding planetary nebulae and galaxies); the black area represents the HII regions sample, and the white area the reflection nebulae sample.

The distribution of f_{ir} is strongly peaked for the HII regions sample between 1 and 1.5%. Correcting for the contribution of the 6.2 μm emission band (as above) yields a fraction of elemental carbon in the form of PAH molecules of (0.4 - 1.5)% in HII regions. The distribution of f_{ir} for the reflexion nebulae is more spread than that of the HII regions and covers the range 1 to 6%, or after correction for the 6.2 μm contribution the range (1.5 - 8)%. These numbers yield an abundance of carbon atoms locked in PAH molecules in the range

$$N_C^{PAH} / N_H \sim (0.2 - 3) \times 10^{-5}$$

4.4.2. Mid-infrared continuum

In principle, a similar analysis could be performed on the underlying continuum. However, the nature of the mid-infrared continuum is still unclear due to a lack of high-resolution spectroscopic data. From the present LRS spectra and recent published spectra (Buss et al., 1990), it is obvious that this continuum is not smooth and, in any case, cannot be approximated by e.g. a modified black-body emission. Possible carriers could be carbon clusters of a few hundred carbon atoms with an infrared spectrum dominated by C ≡ C stretching modes (Allamandola et al., 1989). Vibrational spectra of aromatic carbonaceous compounds (Wdowiak et al., 1988) also show that many bands overlap in the spectral region between 5 and 13 μm. Such bands could account for part of the observed mid-infrared continuum. Clearly further spectroscopic studies are needed to progress on our understanding of this continuum or pseudo continuum.

Since the properties such as the excitation mechanism and absorption cross sections of the species responsible for the mid-infrared continuum are not known, a detailed analysis is not possible. However, their contribution (around 10 μm) to the total infrared flux, f_{ir}^{c}, can be estimated from the numbers listed in Table 1 by

$$f_{ir}^{c} = \frac{F_{LRS1} - F_{PAH}}{F_{IR}}$$

where F_{LRS1} is the flux in the LRS1 band. The histogram of the distribution of f_{ir}^{c} is shown in Fig. 6 (lower panel). A strong peak is found around 1% (in the range 0.5 to 1.5%) both for the HII regions and the reflection nebulae. f_{ir}^{c} is probably a lower limit to the contribution of these species to the infrared flux if account is made for the continuum observed at shorter wavelengths (underneath the 6.2 μm emission feature), and possibly at longer wavelengths. In any case, these numbers shows that the contribution of the mid-infrared continuum to the total infrared flux is comparable or even larger than the contribution of the emission bands.

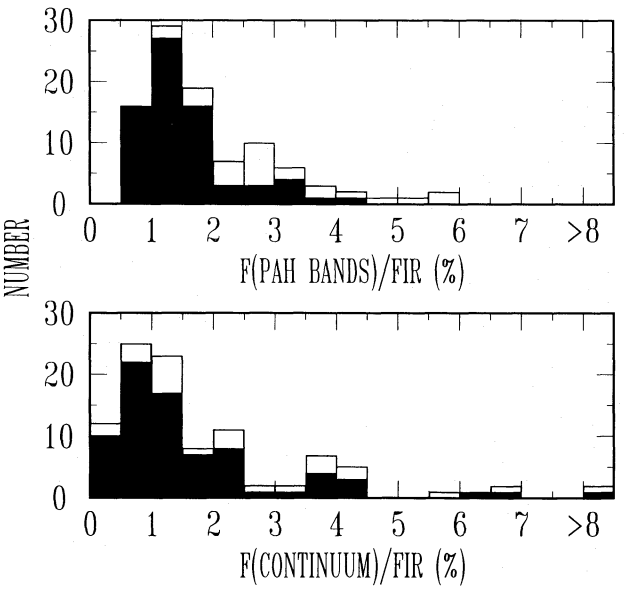

Fig. 6. Histogram showing the distribution of f_{ir} (in percent), the contribution to the total infrared flux of the mid-infrared emission bands at 7.7, 8.6 and 11.3μm (upper panel), and of the mid-infrared continuum between 7.5 and 13.5 μm (lower panel). The black areas and the white areas represent the HII regions and the reflection nebulae, respectively.

4.4.3. Comments

The above values deserve the following comments:

1. The numbers found for compact sources (HII regions and reflection nebulae) are in agreement with previous estimates (Omont, 1986; Allamandola et al., 1989 and Puget and Léger, 1989).

2. The ratio $N_C^{PAH} / N_H \sim (0.2 - 3) \times 10^{-5}$ is significantly lower than the ratio derived by Puget and Léger (1989) for diffuse interstellar clouds. For typical cirrus clouds, $f_{ir} \sim 20\%$ yielding a fraction of elemental carbon in the form of interstellar PAH molecules of about 15% i.e. an order of magnitude higher than in HII regions. Since f_{ir} in this latter case includes both the continuum and the emission bands (no spectroscopic data exist for diffuse clouds; a separation of their respective contributions has still to be done) the quoted number has clearly to be considered as an upper limit. Assuming the continuum and the emission bands contribute about equally (as for the galaxies in our sample), f_C will be of the order of 7%, still a high number as compared with the 1% peak value derived for the HII regions but consistent with the most extreme values encountered in our sample. A likely explanation of this difference could be the destruction of PAH molecules in the harsh radiation field around O and B stars such as in the California Nebula (Boulanger et al., 1989) or the Rosette Nebula (Cox et al., 1990). An alternative explanation could be the fact that an important fraction of the aromatic molecules are condensed onto the grain mantles in the cocoon surrounding the HII regions, and released in the diffuse interstellar medium after absorption of UV photons (Boulanger et al., 1990).

3. It is interesting to note that for the planetary nebulae the mid-infrared flux is dominated by the continuum rather than by the emission bands (see Fig. 4b). This strong continuum is predominantly dust-related emission: the free-free continuum is indeed small with an estimated contribution of 5% to the 12 μm IRAS flux in most of the cases, the maximum contribution being ~ 10% (see also Pottasch, 1982). This could indicate that the species responsible for the mid-infrared continuum are more abundant than the aromatic species in planetary nebulae. The same trend is found for the highly excited HII regions suggesting again that the band carriers (PAHs) are destroyed in strong radiation fields.

5. Conclusions

The main results of this study are:

1. A strong correlation is found between the luminosities of the (7.7 + 8.6) μm and 11.3 μm emission bands from a sample of 77 sources. The spread around the mean value of 8.3 is about 30% (comparable to the errors of the measurements) and the slope of the correlation is nearly unity, confirming that the carriers of these emission features belong to the same class, most likely large aromatic molecules (or PAH molecules). According to recent theoretical calculations, the fact that the (7.7 + 8.6) μm band is about eight times stronger than the 11.3 μm band suggests that in the present sources (HII regions, reflection nebulae and planetary nebulae) the PAH molecules are ionized rather than neutral.

2. The 7.7, 8.6 and 11.3 μm bands represent (40 - 70)% of the total mid-infrared luminosity for the sources studied in this paper.

3. The emission bands tend to become weaker with respect to the underlying continuum in regions with strong radiation fields. A likely explanation could reside in the destruction of the smaller molecular sized compounds (the PAHs) when exposed to intense radiation fields whereas the carriers of the continuum survive.

4. The excitation of the 7.7 and 11.3 μm emission features is due predominantly to photons in the range 91 - 365 nm, as shown by a simple analysis of the relation between the number of UV photons available in this range and the luminosity in these emission bands.

5. The distribution of the abundance number of carbon atoms in PAH molecules, for the sample of HII regions, peaks around 5×10^{-6}. This number includes a correction for the contribution of the 6.2 μm not measured by the IRAS/LRS spectrum. For the reflection nebulae sample, the values are more spread and span the range $(0.2 - 3) \times 10^{-5}$.

6. The continuum observed around 10μm has a similar contribution, of the order of one percent, to the total infrared flux than the emission bands. The nature of the carriers is, however, not known. Higher resolution spectroscopy and laboratory work should help in identifying this component of the interstellar dust.

Acknowledgements. We are grateful to G. Muratorio for his help during the data reduction. It is a pleasure to thank Dr. A. Léger, J. Lequeux and M. Walmsley for helpful remarks on the manuscript. Dr. M. Jourdain de Muizon is thanked for her comments. One of us (A.Z.) acknowledges financial support from the M.R.T.

References

Aitken, D.K., Roche, P.F., 1980, MNRAS **192**, 679
Aitken, D.K., Roche, P.F., 1980, MNRAS **200**, 217
Allamandola, L.J., Tielens, A.G.G.M., Barker, J.R., 1989, ApJS **71**, 733
Boulanger, F., Pérault, M., 1988, ApJ **330**, 964
Boulanger, F., Beichman, C., Désert, F.X., Helou, G., Pérault, M., Ryter, C., 1989, ApJ **332**, 328
Boulanger, F., Falgarone, E., Puget, J.-L., Helou, G., 1990, ApJ **364**, 136
Bregman, J.D., Allamandola, L.J., Tielens, A.G.G.M., Geballe, T.R., Witteborn, F.C., 1989, ApJ **344**, 791
Buss Jr., R.H., Cohen, M., Tielens, A.G.G.M., Werner, M.W., Bregman, J.D., Witteborn, F.C., Rank, D., Sandford, S.A., 1990, ApJ **365**, L23
Caswell, J.L., Haynes, R.F., 1987, A & A **171**, 261
Cohen, M., Allamandola, L.J., Tielens, A.G.G.M., Bregman, J., Simpson, J.P., Witteborn, F.C., Wooden, D., Rank, D., 1986, ApJ **302**, 737
Cohen, M., Tielens, A.G.G.M., Bregman, J., Witteborn, F.C., Rank, D.M., Allamandola, L.J., Wooden, D.H., de Muizon, M., 1989, ApJ **341**, 246
Cox, P., Mezger, P.G., 1989, A & AR **1**, 39
Cox, P., Deharveng, L, Leene, A., 1990, A & A **230**, 181
de Frees, D.J., Miller, D.J., Talbi, D., Pauzat, F., Ellinger, Y, 1992, ApJ submitted
Désert, F.X., Boulanger, F., Puget, J.-L., 1990, A & A **237**, 215
Duley, W.W. and Williams, D.A., 1981, MNRAS **196**, 269
Felli, M., Harten, R.H., 1981, A & A **100**, 42
Fich, M., 1986, AJ **92**, 787
Geballe, T.R., Tielens, A.G.G.M., Allamandola, L.J., Moorhouse, A., Brand, P.W.J.L., 1989, ApJ **341**, 278
Haynes, R.F., Caswell, J.L., Simons, L.W.J., 1978, Aust.J.Phys. Suppl **45**, 1
d'Hendecourt, L., Léger, A., 1988, A & A **180**, L9
IRAS Science Team, 1986, A & AS **65**, 607
IRAS Explanatory Supplement, 1988, eds Beichman, C.A., Neugebauer, G., Habing, H.J., Clegg, P.E., Chester, T.J., NASA RP-1190, chapter IX
Israel, F.P., 1977, A & A **59**, 27
Jourdain de Muizon, M., Cox, P., Lequeux, J., 1990a, A & AS **83**, 337
Jourdain de Muizon, M., d'Hendecourt, L.B., Geballe, T.R., 1990b, A & A **227**, 526
Kurucz, R.L., 1979, ApJS **40**, 1
Léger, A., Puget, J.-L., 1984, A & A **137**, L5
Léger, A., Verstraete, L., d'Hendecourt, L., Défourneau, D., Dutuit, O., Schmidt, W., Lauer, J.C., 1989, Interstellar Dust IAU Symposium n. 135, L.J. Allamandola and A.G.G.M. Tielens, eds. pp. 173-180
Léger, A., d'Hendecourt, L., Défourneau, D., 1989, A & A **216**, 148
Muizon, M. de, Cox, P., Lequeux, J., 1988, A & A **203**, 207
Omont, A., 1986, A & A **164**, 159
Panagia, N., 1973, AJ **78**, 929
Pottasch, S.R., 1982 in Planetary Nebulae, Reidel, p. 193
Puche, D., Zijlstra, A.A., Boettcher, C., Plante, R.L., Wilcots, E.M., Wilkin, F.P., Krause, S., Sergo, S.P., Biermann, G.S., Ge, J., Holliman, J.H., Wu, X., Zhao, J.H., 1988, A & A **206**, 89
Puget, J.-L., Léger, A., 1989, ARA & A **27**, 161
Reich, W., Fürst, E., Steffen, P., Reif, K., Haslam, C.G.T., 1984, A & AS **58**, 197
Rice, W., Lonsdale, C.J., Soifer, B.T., Neugebauer, G., Koplan, E.L., Lloyd, L.A., de Jong, T., Habing, H.J., 1988, ApJS **68**, 91
Roche, P.F., Aitken, D.K., Smith, C.H., 1989, MNRAS **236**, 485
Russell, R.W., Soifer, B.T., and Willner, S.P., 1977, ApJ **217**, L149
Sakata, A., Wada, S. Tanabe, T. and Onaka, T., 1984, ApJ **287**, L51
Sellgren, K., Werner, M.W., Dinerstein, H.L., 1983, ApJ **271**, L13
Simpson, J.P., Rubin, R.H., 1990, ApJ **354**, 165
Verstraete, L., Léger, A., d'Hendecourt, L., Dutuit, O., Défourneau, D., 1990, A & A **237**, 436
Verstraete, L., 1990, Thèse Université Paris VII
Volk, K.M., Cohen, M., 1989a, AJ **98**, 931
Volk, K.M., Cohen, M., 1989b, AJ **98**, 1918
Volk, K.M., Cohen, M., 1990, AJ **100**, 485
Wdowiak, T.J., Flickinger, G.C., and Cronin, J.R., 1988, ApJ **328**, L75
Wildeman, K.J., Beintema, D.A., Wesselius, P.R., 1983, J. British Interplanetary Soc. **36**, 21
Willner, S.P., Soifer, B.T., Russell, R.W., Joyce, R.R., and Gillett, F.C., 1977, ApJ **217**, L121
Wink, J.E., Altenhoff, W., Mezger, P.G., 1982, A & A **108**, 227
Wink, J.E., Wilson, T.L., Bieging, J.H., 1983, A & A **127**, 211
Wood, D.O.S., Churchwell, E., 1989, ApJS **69**, 831
Wouterloot, J.G.A., Brand, J., 1989, A & AS **80**, 149

This article was processed by the author using Springer-Verlag TEX A&A macro package 1991.